Chem. Res. Chinese Universities, 2019, 35(4), 667—673 doi: 10.1007/s40242-019-9014-8

Pd/TiO_2 Nanospheres with Three-dimensional Hyperstructure for Enhanced Photodegradation of Organic Dye

WANG Huan[1,2], XIAO Liguang[2], WANG Chao[1], LIN Bin[1], LYU Sa[1], CHU Xuefeng[1], CHI Yaodan[1], YANG Xiaotian[1*] and WANG Xinyan[3]

1. Jilin Provincial Key Laboratory of Architectural Electricity & Comprehensive Energy Saving, 2. Department of Materials Science, Jilin Jianzhu University, Changchun 130118, P. R. China;

3. State Key Laboratory of Electroanalytical Chemistry, Changchun Institute of Applied Chemistry, Chinese Academy of Sciences, Changchun 130022, P. R. China

Abstract Pd/TiO_2 nanospheres assembled from nanorods with three-dimensional hyperstructure for enhanced photodegradation of organic dye was prepared by a sample solvothermal method. Further, it was used for degradation of methyl orange(MO) under the illumination of visible-light(simulated). The results show that Pd/TiO_2 with 2%(mass fraction) Pd exhibits the noticeable activity in photodegrading of MO. The detailed analysis shows that this enhancement is attributed to the reduction of the rate of electron-hole recombination and surface plasmon resonance of Pd. The high activity and good stability of the obtained Pd/TiO_2 nanospheres make it a promising photocatalyst for solving the environmental pollution problems.

Keywords TiO_2; Pd; Photocatalytic degradation; Surface plasmon resonance

1 Introduction

Titanium dioxide(TiO_2), a significant photocatalyst, has been widely studied by many research groups due to its characteristics including excellent optical activity, high optical stability, nontoxicity and abundant source[1]. However, TiO_2 is a wide band-gap(3.2 eV) semiconductor and therefore can only be excited by ultraviolet(UV) light to perform photo-electrical conversion[2]. While it is known that the UV light is only a small portion of solar light. In this way, most of research works are mainly focused on the methods of narrowing the band gap width in order to extend the absorption of the material into the visible region. These methods include metal or non-metal doping, noble metal coupling and surface sensitization[3—8]. Recently, metal nanostructures with localized surface plasmon resonance(LSPR) effect have been increasingly adopted to narrow the band gap of TiO_2 to enhance its photo-catalytic activity in the visible region[9]. It has been reported that noble metals nanoparticles such as Au, Ag and Pd with surface plasmon resonance(SPR) effect could effectively enhance the absorption of the host material in the visible region[10—13].

The SPR of Pd nanoparticles(NPs) is affected by its size and local environment. In 2003, Kelly *et al*.[14] demonstrated that the refractive index of the substrate had a strong influence on the SPR response region of Pd. Their results show that there was a red shift of about 100 nm in the SPR wavelength of Pd. Moreover, several recent reports have further demonstrated that the SPR response of the Pd NPs can be shifted from the ultraviolet range to the visible-near infrared region(410—800 nm) by varying the size of Pd NPs, indicating that the light absorption efficiency and surface activity can be significantly enhanced by regulating the size and morphology of Pd NPs[13,15]. Therefore, it is reasonable to deduce that the Pd nanostructures may possess the ability to widen the absorption of TiO_2 into the visible region, which paves a new approach and strategy for the preparation of visible light photocatalyst.

In this paper, Pd/TiO_2 nanospheres with three-dimensional hyperstructure were prepared using a facile solvothermal method with tetrabutyl titanate and palladium chloride as source and ethylene glycol as the reducing agent. The photocatalytic activity of the prepared Pd/TiO_2 composite was studied by monitoring the degradation of MO under the illumination of visible light. The results show that the obtained sample exhibited superior photocatalytic activity for degradation of MO. Furthermore, the probable mechanism of enhancement was also discussed.

2 Experimental

2.1 Preparation of Pd/TiO_2 Nanospheres with Three-dimensional Hyperstructure

Pd/TiO_2 nanospheres with three dimensional hyperstructure

*Corresponding author. Email: hanyxt@163.com

Received January 14, 2019; accepted March 8, 2019.

Supported by the National Natural Science Foundation of China(No.51672103), the Science and Technology Development Project of Jilin Province, China(Nos.JJKH20180585KJ, 20190201286JC, 20170101111JC).

were prepared with the solvothermal method[16]. Typically, 1.6 mL of 28.3 mmol/L $PdCl_2$ ethylene glycol solution was added to a beaker containing 15 mL of 0.2 mol/L ethylene glycol tetrabutyl titanate solution. After stirring for 30 min, 15 mL of 5 mol/L NaOH solution was added and the mixture was stirred for 2 h sufficiently. The mixture was transferred to a 50 mL PTFE hydrothermal autoclave and then heated at 200 °C for 20 h to obtain the sample. The sample was filtered using a microporous membrane, then repeatedly washed with 0.2 mol/L HCl and water subsequently. The obtained powder was dried at 80 °C overnight, then annealed in air at 500 °C for 2 h and labelled as 2.0% Pd/TiO_2(the mass fraction of Pd was 2.0%). Under the similar conditions, TiO_2, 1.0% Pd/TiO_2, 1.5% Pd/TiO_2, and 2.5% Pd/TiO_2 samples were also prepared.

2.2 Characterization

The crystal structure of the samples was characterized using an X-ray diffractometer(Rigaku D/Max 2550, Rigaku Co., Ltd., Japan) with Cu $K\alpha$ radiation(λ=0.154056 nm) at 40 kV and 200 mA. The morphology and structure of the products were measured by a filed-emission scanning electron microscope (FESEM, JSM-7610F) and a transmission electron microscope (TEM, Fei Tecnai G2 F20 S-TWIN). The chemical components of the samples were obtained using an energy dispersive spectrometer(EDS) attached with FESEM. X-Ray photoelectron spectroscopy(XPS) analysis was carried out on an ESCALAB MKII photoelectron spectrometer with Al $K\alpha$ radiation. Ultraviolet visible(UV-Vis) absorption and UV-Vis diffuse reflectance spectra(using $BaSO_4$ as the reference) were collected on a Shimadzu UV-2600 spectrophotometer. The Brunauer-Emmett- Teller(BET) surface area and porosity of the samples were determined by using a Micromeritics ASAP 2020 nitrogen adsorption apparatus. The electron paramagnetic resonance(EPR) and EPR spin trapping spectra in suspensions were characterized with a JES-FA 200 Spectrophotometer operating at 9.4 kHz magnetic field modulation with visible-light irradiation. The photoelectric conversion performance was obtained at room temperature using a photoelectrochemical(PEC) cell at several on-off irradiation cycles in Na_2SO_4 aqueous solutions under visible light irradiation.

2.3 Evaluation of Photocatalytic Activity

The photocatalytic activity was studied by photodegradation of MO (10 mmol/L, 50 mL) in the presence of 50 mg suspended photocatalyst using absorption spectroscopy. The suspension was stirred in the dark for 30 min to achieve an equilibrium of adsorption of MO on the photocatalyst. A 300 W xenon lamp(PLS-SXE-300, Beijing Perfectlight Technology Co., Ltd.) equipped with a UV filter(λ>420 nm) was applied as the light source. 1 mL of the dispersion was pipetted at a certain time interval and the solid powders were removed by centrifugation to obtain solution for analysis. The UV-Vis spectrum of the solution was collected and the concentration of MO was calculated according to the characteristic absorbance peak intensity of MO at 463 nm.

3 Results and Discussion

3.1 Characterization of Morphology and Structure of Pd/TiO_2 Nanospheres with Three-dimensional Hyperstructure

XRD patterns of the obtained TiO_2 and Pd/TiO_2 composites with different mass fractions of Pd are shown in Fig.1. It is shown that all the samples show significant diffraction peaks at 2θ=25.2°, 37.8°, 48.1°, 53.8°, 55.1°, 62.7°, 68.7°, 70.3°, 75.0° and 82.6°, corresponding to the (101), (004), (200), (105), (211), (204), (116), (220), (215), (224) diffractions of anatase TiO_2(JCPDS No.21-1272)[17]. Due to the low Pd concentration, no diffraction peak of Pd is observed in the XRD patterns of Pd/TiO_2 composites.

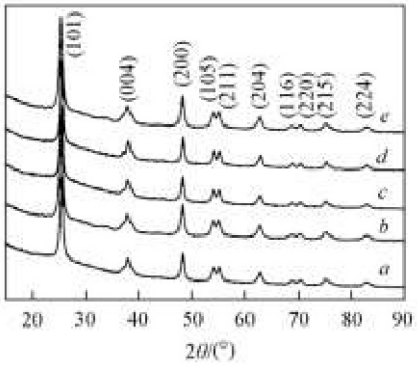

Fig.1 XRD patterns of TiO_2(*a*) and the 1.0% Pd/TiO_2(*b*), 1.5% Pd/TiO_2(*c*), 2.0% Pd/TiO_2(*d*) and 2.5% Pd/TiO_2(*e*) nanospheres

The morphology, structure and elemental distribution of Pd/TiO_2 composites were characterized by means of SEM, TEM and HRTEM. Fig.2 shows the SEM image and enlarged SEM images of the 2.0% Pd/TiO_2 composites. It can be seen that it exhibits the hierarchical spherical structures with diameters in the range of 2—4 μm. In the high-resolution SEM image [Fig.2(C)], it is shown that the nanospheres are composed of one-dimensional nanorods with 3D hierarchical structure and the diameters of nanorods are several nanometers. The HAADF-STEM and elemental mapping images[Fig.2(D)—(G)] of the 2.0% Pd/TiO_2 composites clearly show the existence of Ti, O and Pd element in the Pd/TiO_2 composites, which agrees well with the XPS results.

The TEM and HRTEM images of the Pd/TiO_2 composite are shown in Fig.3. From the TEM images[Fig.3(A) and (B)], it can be clearly seen that the spherical Pd/TiO_2 composite consists of a solid core and surrounding nanorods. The HRTEM image[Fig.3(C)] shows that the diameter of the nanocrystals was about 2—5 nm. The lattice space of nanocrystals marked with a red circle is 0.35 nm, which is belonged to the (101) crystal plane of TiO_2. The lattice space of the nanocrystals in the area marked with a green elliptical line is 0.23 nm, which agrees well with the (111) crystal plane of the Pd NPs, indicating that the Pd NPs were successfully prepared by the reduction of glycol under alkaline conditions[18].

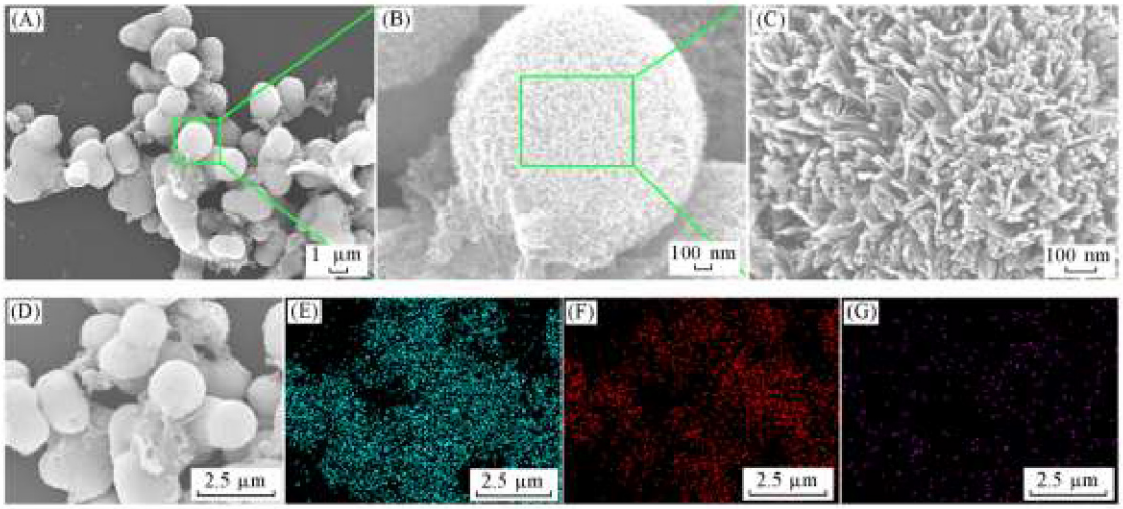

Fig.2 SEM images(A—C), HAADF-STEM image(D) and elemental mapping images of Ti(E), O(F) and Pd(G) of the 2.0% Pd/TiO_2 nanospheres

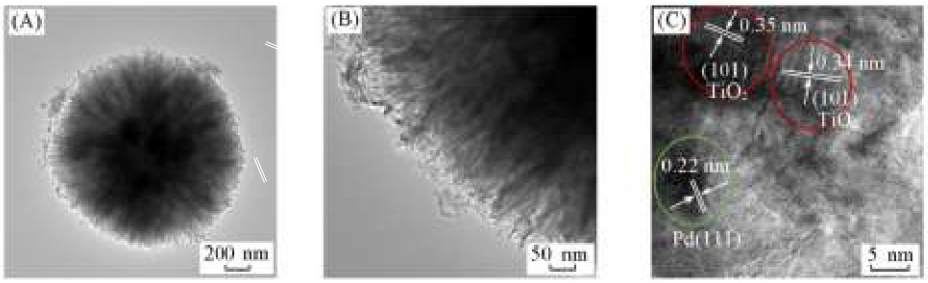

Fig.3 TEM(A, B) and HRTEM(C) images of the 2.0% Pd/TiO_2 nanospheres

The composition and chemical state of the 2% Pd/TiO_2 composites were further investigated by XPS. From the survey XPS spectrum[Fig.4(A)], the peaks of Ti, O and C could be obviously detected. The peak of C is believed to be mainly caused by the adsorption of carbon impurities on the sample surface. The high-resolution Ti_{2p} spectrum of the 2% Pd/TiO_2 composites[Fig.4(B) curve *a*] consists of two characteristic peaks of E_b at 458.2 eV($Ti_{2p_{3/2}}$) and 464.1 eV($Ti_{2p_{1/2}}$). The E_b of $Ti_{2p_{1/2}}$ and $Ti_{2p_{3/2}}$ of the 2.0% Pd/TiO_2 composites are slightly red shifted, comparing with that at 464.5 and 458.8 eV for

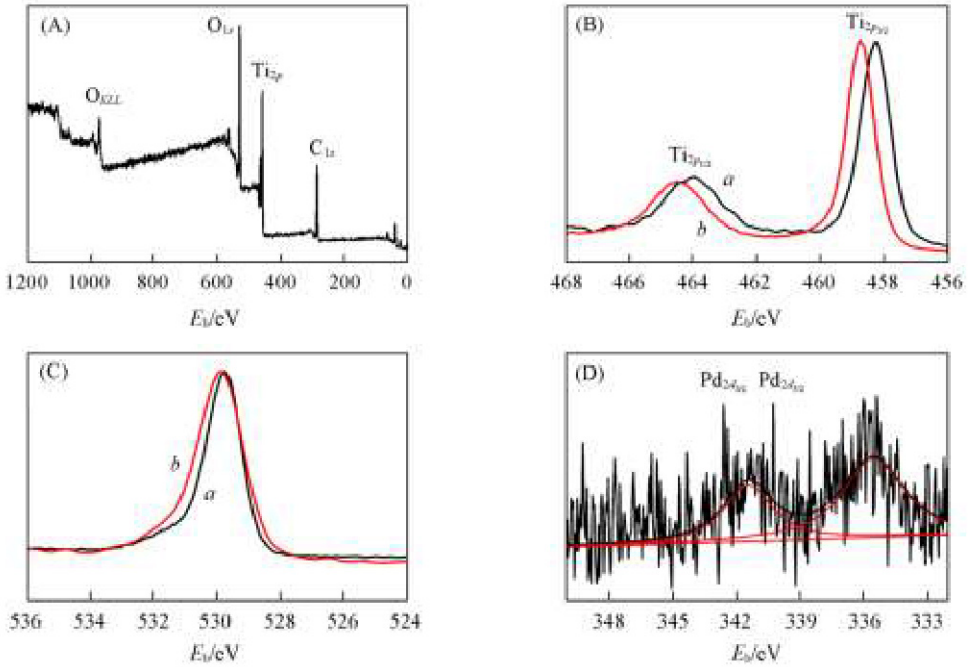

Fig.4 Survey(A), Ti_{2p}(B), O_{1s}(C) and Pd_{3d}(D) XPS spectra of the TiO_2 and 2.0% Pd/TiO_2 nanospheres

(A), (D) 2.0% Pd/TiO_2; (B), (C) *a*. 2.0% Pd/TiO_2; *b*. TiO_2.

pure TiO_2[Fig.4(B) curve *b*], which is possibly caused by the strong electronic interaction between Pd and TiO_2[19]. The O_{1s} XPS peak of the 2.0% Pd/TiO_2 composites[Fig.4(C) curve *a*] is broaden and also shifts to the lower binding energy in comparing with the O_{1s} peak of as-prepared TiO_2 sample. The high resolution Pd_{3d} XPS spectrum[Fig.4(D)] shows two peaks of $Pd_{3d_{3/2}}$ and $Pd_{3d_{5/2}}$ at 335.6 and 341.5 eV, respectively, which can be attributed to Pd^0, indicating the existence of Pd^0 NPs[20].

The N_2 adsorption-desorption isotherm of the 2% Pd/TiO_2 composites[Fig.5(A)] exhibits type IV isotherm with an H3 hysteresis loop in a relative pressure range of 0.4—1.0[16], indicating the presence of mesopores in the 2% Pd/TiO_2 composites. The H3 hysteresis loop associates with the textural larger pores, which is probably caused by the aggregation of nanorods into 3D hierarchical structure. The pore diameter distribution[Fig.5(B)] of the 2% Pd/TiO_2 composites also demonstrates the existence of mesopores in the sample and the pore-size are mainly distributed in the range of 2—50 nm. In addition, the N_2 adsorption-desorption isotherm[Fig.5(A)] of the TiO_2 shows that it is in aporate structure. The BET surface areas of the 2% Pd/TiO_2 composites were calculated to be 57.04 m^2/g.

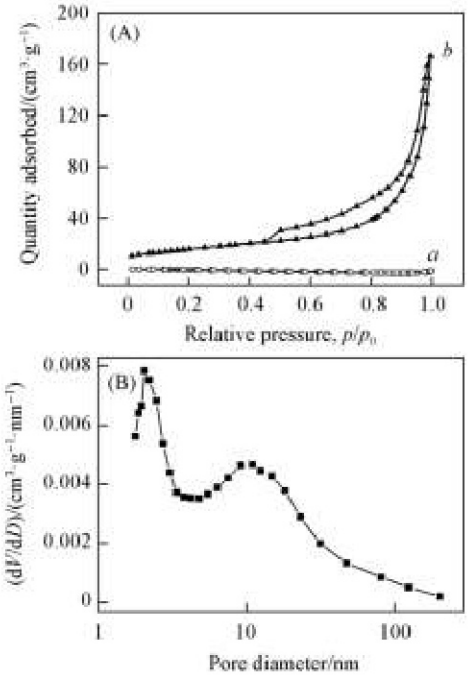

Fig.5 Nitrogen adsorption-desorption isotherms of the TiO_2(*a*) and 2%Pd/TiO_2 nanospheres(*b*)(A) and pore diameter distribution of the 2% Pd/TiO_2 nanospheres(B)

3.2 Photocatalytic Properties of the Spherical 3D Hierarchical Pd/TiO_2 Composites

The optical absorption of the TiO_2 and Pd/TiO_2 composites with different Pd contents were investigated by UV-Vis diffuse reflectance spectra(Fig.6). The as-prepared TiO_2 shows ultraviolet absorption band edges of about 385 nm. As shown in the curve of Pd/TiO_2 composites, a red shift of the absorption band edges occurs compared with the curve of pure TiO_2, which may be attributed to the presence of Ti^{3+} or oxygen vacancies in Pd/TiO_2 composites and the decreasing of the band gap compared with pure TiO_2. The strong and broad visible light absorption peak in the range of 400—550 nm is also observed for all Pd/TiO_2 samples, which is assumed to be caused by the SPR absorption of Pd NPs. This phenomenon has been confirmed by previous reports[21—23]. In this work, the LSPR intensity of absorption increases with increasing the content of Pd. Meanwhile, the absorption intensity gradually reaches saturation when the Pd content reaches 2.0%. The SPR effect of Pd NPs extends the absorption range of the Pd/TiO_2 composites into the visible light region, which effectively improves the utilization efficiency of the sunlight. In order to examine the photoelectric conversion of the photoactive samples, the time-resolved photocurrent experiments were carried out[24].

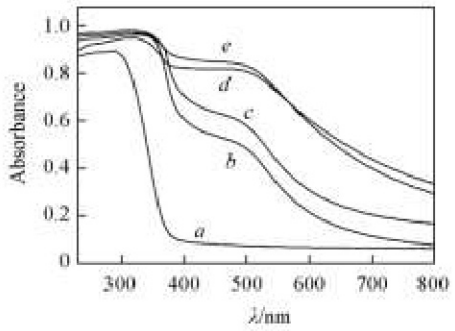

Fig.6 UV-Vis diffuse reflectance spectra of the as-prepared TiO_2(*a*), 1.0%Pd/TiO_2(*b*), 1.5%Pd/TiO_2(*c*), 2.0%Pd/TiO_2(*d*) and 2.5%Pd/TiO_2(*e*) nanospheres

The EPR spectra of samples were recorded at ambient temperature, and the results are shown in Fig.7. The 2.0% Pd/TiO_2 composite shows a strong signal(g=2.003), while the TiO_2 displays no EPR signal. According to previous research, the EPR signal at g=2.003 is caused by oxygen vacancies trapping electrons[25]. However, no representative signal, with the principle values $g_{1,2}$=1.990 and g_3=1.962 of the anatase phase, of Ti^{3+} is shown here, which suggests the absence of Ti^{3+} in the Pd/TiO_2 composites[26].

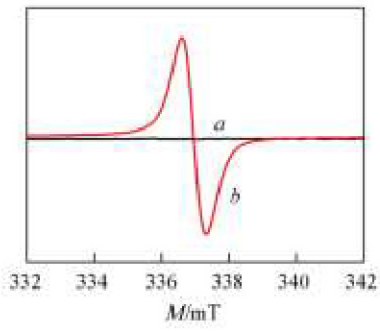

Fig.7 EPR spectra of the TiO_2(*a*) and 2.0% Pd/TiO_2 composites(*b*)

Fig.8 shows the *I-t* curves for as-prepared TiO_2 and Pd/TiO_2 composites with different Pd contents over several on-off intermittent irradiation cycles. Because of the large band gap and the rapid electron-hole recombination for TiO_2,

the photogenerated carriers cannot be efficiently separated and transferred. Thus the photocurrent response of TiO_2 is the lowest.

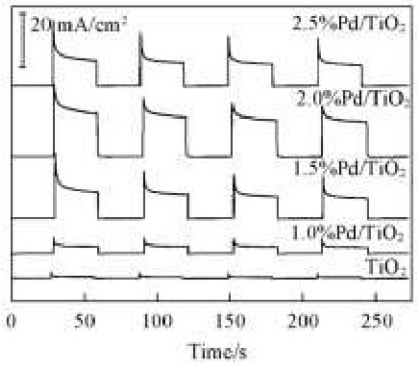

Fig.8 Photocurrent curves of TiO_2 and Pd/TiO_2 composites

The experiments were carried out by switching the visible light source every 50 s at a potential of 0.2 V(*vs*. Ag/AgCl) in Na_2SO_4 aqueous solutions.

Interestingly, after the Pd NPs were *in-situ* introduced into TiO_2, the photocurrent response intensity was significantly increased. With the increase of the Pd content, the photocurrent response intensity is gradually increased. When the Pd content reaches 2.0%, the intensity shows the maximum value and then decreases slightly after further increasing the amount of Pd in the sample. According to the experiments, the photocurrent response of 2.0% Pd/TiO_2 is about 5 times higher than that of 1.0% Pd/TiO_2.

The photocatalytic activity of different as-prepared samples were evaluated by the degradation of the MO dye. Before the light irradiation, the reaction system was placed in the dark for 30 min to equilibrate the adsorption of MO on the photocatalyst. Typical real-time absorption spectrum of MO during the photocatalytic process on all samples are shown in Fig.9(A) and Fig.S1(see the Electronic Supplementary Material of this paper). The real-time concentration changes(c_t/c_0, c_t is the concentration at time t, c_0 is the initial concentration, c_0=10 mg/L) of MO was determined by means of the normalized absorption value(A/A_0, λ=463 nm) according to the Beer-Lambert law at the given time intervals. Fig.9(B) shows the degradation dynamic curves of MO over the TiO_2 and Pd/TiO_2 composites with different content of Pd at the given time intervals. Obviously, MO solution was hardly degraded over TiO_2 under visible light irradiation. This is because TiO_2 can not be excited by visible light irradiation. After the introduction of Pd NPs, the TiO_2 light absorption range can be extended into the visible light region, and the absorption intensity can be significantly increased.

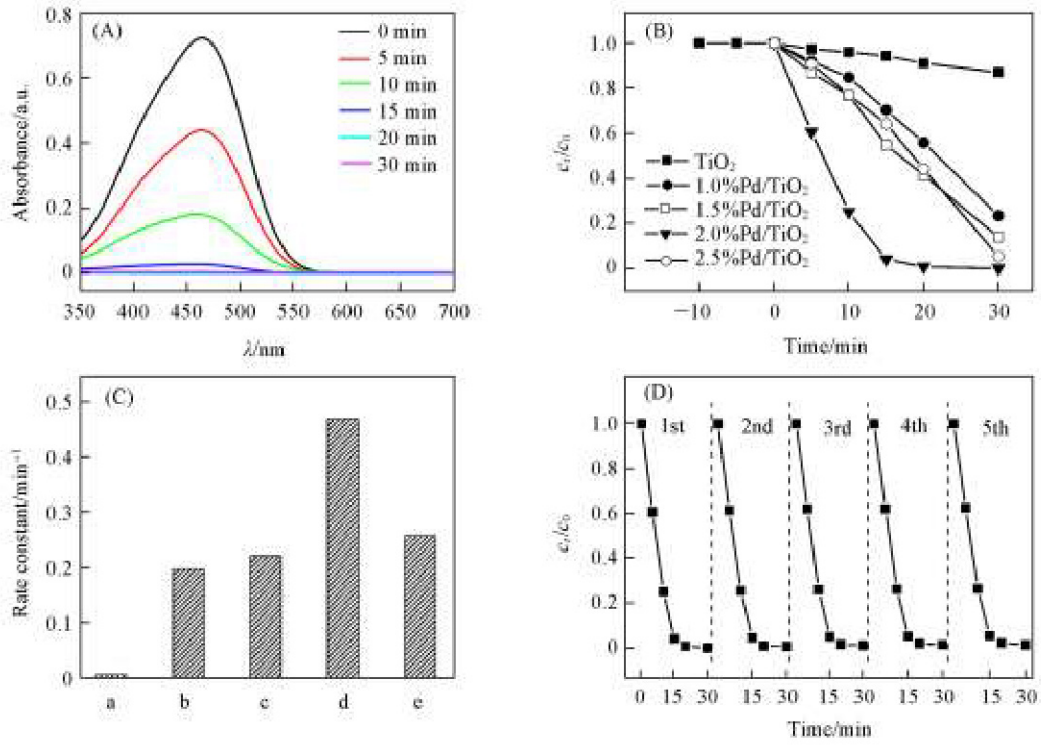

Fig.9 Typical real-time absorption spectra of MO on 2.0% Pd/TiO_2 nanospheres(A), photocatalytic degradation of MO in the presence of different photocatalysts under the irradiation of visible light(B), comparison of rate constants(k_R) of the obtained photocatalysts for MO degradation(C) and five successive photoreductive dynamic curves of MO over 2.0% Pd/TiO_2 photocatalyst under visible-light irradiation(D)

(C) a. TiO_2; b. 1.0% Pd/TiO_2; c. 1.5% Pd/TiO_2; d. 2.0% Pd/TiO_2; e. 2.5% Pd/TiO_2.

The optimal photocatalytic performance was achieved when the solution with 2.0% Pd/TiO_2 composites as catalyst was irradiated for 10 min and 80% of MO was degraded under the illumination of visible light. But the degradation efficiency of MO is slightly decreased with the 2.5% Pd/TiO_2 composites as catalyst, which may be due to the ineffective electron-hole

separation. Furthermore, Since the photocatalytic oxidation process follows a Pseudo-first-order reaction[27], the corresponding degradation rate constant(k_R) were calculated by $\ln(c_0/c_t)=k_R t$, and the results are shown in Fig.9(C). Compared with other catalysts(TiO_2: k_R=0.006 min^{-1}; 1.0%Pd/TiO_2: k_R=0.198 min^{-1}; 1.5%Pd/TiO_2: k_R=0.221 min^{-1}; 2.5%Pd/TiO_2: k_R=0.258 min^{-1}), the 2.0%Pd/TiO_2 photocatalyst(k_R=0.470 min^{-1}) possesses the highest catalytic activity. The main reasons can be summarized as follows: (1) with the increase of Pd content, the band gap narrowing and SPR effect effectively enhanced the transfer and separation of photo electron-hole pairs and further would improve the photocatalytic efficiency[21]. (2) The spherical 3D hierarchical structure had a large BET surface area and therefore many catalytic active sites, which can further enhance its photocatalytic activity[16].

The stability of the prepared photocatalyst was characterized through measuring the Pd/TiO_2 photocatalytic degradation efficiency of MO[Fig.9(D)]. After each cycle, the photocatalyst was centrifuged, washed several times and then vacuum dried again for further usage. After 5 cycles, no obvious efficiency degradation was observed, which shows that the as-prepared sample is suitable to be recycled and can be practically applied.

Generally, the EPR spin trapping technique is used to probe reactive oxidizing species such as superoxide anion radical($O_2^{\bullet-}$), hydroxyl(OH), hydrogen peroxide(H_2O_2), etc. Here the EPR spectra were detected in methyl alcohol and aqueous solution containing the Pd/TiO_2 particles with DMPO spin-trapping reagent under visible light irradiation, and the results are shown in Fig.10. No signal for the DMPO-$^{\bullet}$OH adducts(Fig.10 curve *a*) was detected; while the DMPO-$O_2^{\bullet-}$ adducts with 4-line characteristic signal(Fig.10 curve *b*) were observed in the irradiated system, indicating that $O_2^{\bullet-}$ played the important role in this system[28,29].

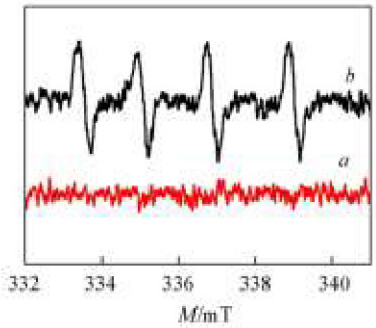

Fig.10 EPR spectra of the 2.0%Pd/TiO_2 composites under visible light irradiation

a. DMPO-$^{\bullet}$OH; *b*. DMPO-$O_2^{\bullet-}$.

Here, the enhanced photocatalytic activity mechanism of Pd/TiO_2 composites is proposed to better explain the photocatalytic degradation process of MO(Fig.11). The energy levels of the conduction band and valence band of TiO_2 are –4.21 and –7.41 eV, respectively[30]. The Fermi level of Pd is about at –5.22 eV. Thus, the Schottky barrier will be formed at the interface of Pd/TiO_2, and the barrier height was calculated to be 1.10 eV[20]. Because of the LSPR of Pd NPs, the photo-excited electrons in the Pd NPs a generated under the illumination of visible light, which makes the photogenerated electrons in Pd possess the sufficient energy to overcome the Schottky barrier and further transfer into the conduction band of TiO_2, thereby retarding the electron-hole(e-h^+) recombination process. These transferred electrons will further diffuse to the surface of TiO_2 and can be captured by the adsorbed oxygen molecules to form superoxide radicals($O_2^{\bullet-}$), which will further contribute to decompose MO[22,31,32].

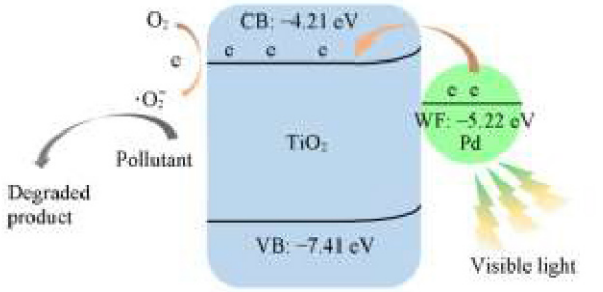

Fig.11 Proposed photocatalytic mechanism over Pd/TiO_2 nanospheres under the irradiation of visible light

4 Conclusions

Pd/TiO_2 nanospheres with three-dimensional hyperstructure were prepared by an effective solvothermal method. Among the as-prepared TiO_2 and Pd/TiO_2 with different Pd contents, the 2.0% Pd/TiO_2 composites exhibited the highest photocatalytic activity and excellent recycle stability in the degradation of MO under visible light irradiation. This can be attributed to two reasons: (1) the LSPR of Pd nanoparticles improves transfer of the photo-excited electrons in the Pd nanoparticles; (2) the 3D hierarchical structure has a large surface area and many surface active sites, which facilitate the rapid reaction. The excellent spherical 3D hierarchical structure of Pd/TiO_2 composites has very bright prospects in the practical applications for solving water pollution and other environmental problems.

Electronic Supplementary Material

Supplementary material is available in the online version of this article at http://dx.doi.org/10.1007/s40242-019-9014-8.

References

[1] Daghrir R., Drogui P., Robert D., *Industrial & Engineering Chemistry Research*, **2013**, *52*, 3581

[2] Pelaez M., Nolan N. T., Pillai S. C., Seery M. K., Falaras P., Kontos A. G., Dunlop P. S. M., Hamilton J. W. J., Byrne J. A., Oshea K., Mohammad H., Dionysiou D. D., *Applied Catalysis B: Environmental*, **2012**, *125*, 331

[3] Seh Z. W., Liu S., Low M., Zhang S. Y., Liu Z., Mlayah A., Han M. Y., *Adv. Mater.*, **2012**, *24*, 2310

[4] Jiang B., Hou Z., Tian C., Zhou W., Zhang X., Wu A., Tian G., Pan K., Ren Z., Fu H., *CrystEngComm*, **2013**, *15*, 5821

[5] Kobosko S. M., Jara D. H., Kamat P. V., *ACS Appl. Mater. Interfaces*, **2017**, *9*, 33379

[6] Duan H., Wang Z., Cui L., Lin B., Zhou Y., *Industrial & Engineering Chemistry Research*, **2018**, *57*, 12358

[7] Zhang C., Zhou Y., Bao J., Sheng X., Fang J., Zhao S., Zhang Y., Chen W., *ACS Applied Materials & Interfaces*, **2018**, *10*, 18796
[8] Deng Q. R., Xia X. H., Guo M. L., Gao Y., Shao G., *Materials Letters*, **2011**, *65*, 2051
[9] Ayati A., Ahmadpour A., Bamoharram F. F., Tanhaei B., Manttari M., Sillanpaa M., *Chemosphere*, **2014**, *107*, 163
[10] Gupta B., Melvin A. A., Matthews T., Dash S., Tyagi A. K., *Renewable and Sustainable Energy Reviews*, **2016**, *58*, 1366
[11] Wang X., Wu T., Wang H., Su X., *Materials Research Bulletin*, **2016**, *73*, 423
[12] Zhang Q., Ye J., Tian P., Lu X., Lin Y., Zhao Q., Ning G., *RSC Advances*, **2013**, *3*, 9739
[13] Lacerda A. M., Larrosa I., Dunn S., *Nanoscale*, **2015**, *7*, 12331
[14] Kelly K. L., Coronado E., Zhao L. L., Schatz George C., *J. Phys. Chem. B*, **2003**, *107*, 66
[15] Leong K. H., Chu H. Y., Ibrahim S., Saravanan P., *Beilstein J. Nanotechnol*., **2015**, *6*, 428
[16] Li H., Yu H., Sun L., Zhai J., Han X., *Nanoscale*, **2015**, *7*, 1610
[17] Bai X., Lv L., Zhang X., Hua Z., *Journal of Colloid and Interface Science*, **2016**, *467*, 1
[18] Xu Y., Zhang C., Zhang L., Zhang X., Yao H., Shi J., *Energy & Environmental Science*, **2016**, *9*, 2410
[19] Tan D., Zhang J., Shi J., Li S., Zhang B., Tan X., Zhang F., Liu L., Shao D., Han B., *ACS Applied Materials & Interfaces*, **2018**, *10*, 24516
[20] Zhou W., Guan Y., Wang D., Zhang X., Liu D., Jiang H., Wang J., Liu X., Liu H., Chen S., *Chemistry: An Asian Journal*, **2014**, *9*, 1648
[21] Yang W., Xiong Y., Zou L., Zou Z., Li D., Mi Q., Wang Y., Yang H., *Nanoscale Research Letters*, **2016**, 11
[22] Yu L., Li D., *Catalysis Science & Technology*, **2017**, *7*, 635
[23] Xu C., Huang W., Li Z., Deng B., Zhang Y., Ni M., Cen K., *ACS Catalysis*, **2018**, *8*, 6582
[24] Li H., Gan S., Wang H., Han D., Niu L., *Adv. Mater*., **2015**, *27*, 6906
[25] Shah M. W., Zhu Y., Fan X., Zhao J., Li Y., Asim S., Wang C., *Scientific Reports*, **2015**, *5*, 15804
[26] Zuo F., Wang L., Wu T., Zhang Z., Borchardt D., Feng P., *J. Am. Chem. Soc.*, **2010**, *132*, 11856
[27] Li H., Wu T., Cai B., Ma W., Sun Y., Gan S., Han D., Niu L., *Applied Catalysis B: Environmental*, **2015**, *164*, 344
[28] Khachatryan L., Vejerano E., Lomnicki S., Dellinger B., *Environ. Sci. Technol.*, **2011**, *45*, 8559
[29] Fenoglio I., Greco G., Livraghi S., Fubini B., *Chem. Eur. J*., **2009**, *15*, 4614
[30] Zhang R., Wang H., Tang S., Liu C., Dong F., Yue H., Liang B., *ACS Catalysis*, **2018**, *8*, 9280
[31] Fan Y., Ma W., Han D., Gan S., Dong X., Niu L., *Adv. Mater.*, **2015**, *27*, 3767
[32] Wang X., Wang H., Yang X., Su X., *Chem. Res. Chinese Universities*, **2016**, *32*(4), 661